

Article

Enhancing Throughput in IoT Networks: The Impact of Active RIS on Wireless Powered Communication Systems

Iqra Hameed ¹ and Insoo Koo ^{2,*}

¹ Department of Electronic Engineering, Hanyang University, Seoul 04763, Republic of Korea; engriqrahameed056@gmail.com

² Department of Electrical, Electronic and Computer Engineering, University of Ulsan, Ulsan 44610, Republic of Korea

* Correspondence: iskoo@ulsan.ac.kr

Abstract: This paper investigates the potential of active reconfigurable intelligent surfaces (RIS) to enhance wireless-powered communication networks (WPCNs), addressing the evolving connectivity needs of the internet of things (IoT). Active RIS, capable of amplifying and reflecting signals, offers a solution to surpass the limitations of passive RIS, such as double-fading attenuation, aiming to significantly improve network throughput and coverage. Our research focuses on exploiting the amplification capabilities of active RIS to boost the overall network sum throughput, engaging in a comprehensive optimization of critical network parameters, including time allocation, reflection coefficients, and phase shift matrices specific to active RIS. The formulated problem is non-convex and highly complex due to the coupling of optimization variables. We employed a successive convex approximation algorithm to solve the throughput maximization problem by converting the non-convex constraints into approximated convex constraints and solving them iteratively. Through extensive simulations, we demonstrate that our active RIS-assisted network substantially outperforms networks facilitated by passive RIS, marking a significant advancement in WPCN performance. These findings underscore the potential of active RIS technology in realizing the full capabilities of IoT connectivity.

Keywords: active reconfigurable intelligent services; wireless power transfer (WPT); wireless information transfer (WIT); iterative convex optimization; successive convex approximation



Citation: Hameed, I.; Koo, I. Enhancing Throughput in IoT Networks: The Impact of Active RIS on Wireless Powered Communication Systems. *Electronics* **2024**, *13*, 1402. <https://doi.org/10.3390/electronics13071402>

Academic Editor: Ic-Pyo Hong

Received: 27 March 2024

Revised: 3 April 2024

Accepted: 7 April 2024

Published: 8 April 2024



Copyright: © 2024 by the authors. Licensee MDPI, Basel, Switzerland. This article is an open access article distributed under the terms and conditions of the Creative Commons Attribution (CC BY) license (<https://creativecommons.org/licenses/by/4.0/>).

1. Introduction

The rapid evolution of communication technologies has revolutionized the internet of things (IoT), in which thousands of devices connect and communicate with each other and the wider world. Cellular networks have emerged as the primary infrastructure for connecting IoT devices. They provide widespread coverage and reliable connectivity, making them an essential component of the IoT ecosystem [1]. Although 5G and beyond 5G (B5G) technologies are on the horizon, their global implementation is still developing. These technologies promise significant advances in speed, latency, and connectivity. Despite their potential, 5G and B5G technologies deliver lower data rates and face challenges in supporting advanced forms of communication. These limitations highlight the need for more advanced solutions [2].

Researchers are already considering sixth-generation (6G) technology as a potential solution to the shortcomings of 5G and B5G. 6G is envisioned to offer unprecedented capabilities in terms of speed, capacity, and new communication paradigms. Nevertheless, the potential increase in energy consumption is one of the significant concerns with the advent of more advanced technologies. This can have environmental and economic implications. IoT devices often operate on battery power, and their limited lifespan can pose challenges, particularly in scenarios where continuous operation is critical. Energy consumption and

battery lifespan issues impact the ability to maintain a seamless and intelligent connection among IoT devices. This is crucial for applications where real-time data and communication are essential. Energy-efficient communication refers to strategies and technologies that maximize energy efficiency and environmental impact in communication technology [3,4].

The network's lifetime can be extended through the promising technique of wireless energy harvesting. This method can offer wireless networks an essentially boundless power source by gathering energy from the surrounding environment. There is an increasing focus on wireless-powered communication networks (WPCNs) as an economical and energy-efficient solution. These networks are designed to deliver appropriate energy, enable adaptable wireless energy transfer, and facilitate efficient communication [5–8].

1.1. Wireless Powered Communication Networks

In WPCNs, a hybrid access point (H-AP) engages in simultaneous wireless energy transfer (WET) to, and wireless information transfer (WIT) from, multiple wireless nodes. The H-AP acts as the principal energy source, emitting electromagnetic power to nodes within the network's perimeter. Within this framework, a "harvest-then-transmit" paradigm is predominantly employed, indicating that the nodes lack autonomous energy storage. Instead, these entities accumulate and store energy conveyed by the H-AP, utilizing this harvested power for subsequent information transmission towards the H-AP in the uplink phase. This mechanism obviates the necessity for traditional electrochemical batteries, thereby diminishing maintenance requisites [6,9]. The interaction between communication and energy transfer is integral to a WPCN. The energy requirements of wireless devices (WDs) to meet their uplink communication quality standards determine the strategy for downlink energy transfer. On the other hand, uplink information transmission is causally constrained by the amount of energy available at each WD after undergoing energy harvesting through wireless power transfer (WPT) in the downlink. Consequently, coordinating information and energy transmissions is essential for preventing interference and optimizing the overall system performance [10]. Optimal time allocation for WET and WIT is crucial for ensuring the desired minimum requirements in WPCNs. The distribution of time slots between WET and WIT significantly impacts the network's performance. Furthermore, the efficiency of wireless energy transfer diminishes with increased distance from the H-AP due to augmented path loss and attenuation, leading to reduced energy reception by distant devices. Advances such as relay cooperation and massive multiple-input multiple-output (MIMO) technologies have been proposed to enhance energy and spectral efficiencies and increase the range of WIT of the network.

Recent works have focused on throughput analysis of wireless-powered IoT networks in various scenarios [11–14] in different scenarios. Liu et al. proposed an optimal transmission policy that maximizes the throughput of a mobile WPCN by optimally pairing the energy consumption of one transmission with the energy harvesting probability, considering the mobility of the energy access point and data access point and the resultant variable distances. Their approach introduces a two-layer algorithm that effectively addresses the joint optimization problem, dividing the network into energy-sufficient and energy-limited states [11]. Zheng et al. investigated throughput maximization by optimizing time, power, and channel allocation by introducing two algorithms for a wireless-powered IoT system: a generated data packets-based throughput maximization (GDPTM) algorithm for short-term throughput maximization when IoT nodes have sufficient energy, and a deep deterministic policy gradient (DDPG)-based multi-node resource allocation (DMRA) algorithm for resource allocation when energy is insufficient [12]. Tang et al. presented a two-stage design method to optimize energy efficiency in a millimeter-wave-based WPCN with an H-AP and multiple IoT devices, addressing non-convex optimization through stable grouping, optimal antenna allocation using the principle of two-side exchange stability (TES), and optimal sub-time slot and bandwidth allocations using the Dinkelbach algorithm and the Lagrange dual method [14]. Nonetheless, the real-world implementation of these technolo-

gies faces challenges related to power usage, expenses associated with hardware, and the complexities of signal processing [8].

1.2. Reconfigurable Intelligent Surface-Aided Wireless Networks

Reconfigurable intelligent surfaces (RISs) are a promising technology that may address the escalating demands of wireless networks, particularly in the context of advances in 5G and B5G [15]. These RISs are designed as artificial planar structures equipped with integrated electronic circuits that enable them to adapt and manipulate incoming electromagnetic waves in a controlled manner. RISs are constructed from low-profile, lightweight, and cost-effective materials, allowing them to be easily shaped with desired geometries. This facilitates their deployment on various surfaces within various environments, including building facades, walls, and ceilings. The incorporation of RISs in wireless networks offers several advantages. The propagation from transmitters to receivers can be optimized by intelligently steering the signals reflected by the RIS, significantly enhancing the resulting signal quality. This, in turn, results in higher spectral efficiencies than current wireless systems [16]. Furthermore, RISs can be pivotal in mitigating co-channel interference, a critical concern in densely populated urban environments with a high concentration of communication terminals. This is achieved by selecting distinct propagation paths for interfering signals, enhancing overall network performance [17]. Through the progression in metasurface technology and micro-electro-mechanical systems (MEMS), RIS components can undergo real-time modifications utilizing adjustable phase shifters [18]. This capacity for dynamic alteration facilitates the adaptability of RIS to diverse communicative scenarios and fluctuating environmental contexts.

1.2.1. Passive RIS-Aided Networks

Most research efforts focused primarily on passive RISs [19–26], equipped with passive loads (positive resistance), that reflect the incident signal with the desired phase shift and reflection gain no larger than one. In contrast to conventional active relays, passive RIS operates without expensive transmit/receive radio-frequency (RF) chains [27]. This characteristic leads to a substantial decrease in power consumption. By leveraging passive elements, passive RISs can manipulate and redirect electromagnetic waves without requiring energy-intensive electronic components. This makes passive RISs an appealing technology for enhancing wireless communication networks, particularly in scenarios where power efficiency and cost-effectiveness are paramount considerations. Furthermore, passive RISs operate in a full-duplex mode without amplification, noise processing, or self-interference management. Shi et al. explored the benefits of integrating a passive RIS into a WPCN to enhance WET and WIT efficiencies [8]. Their research focused on maximizing the secrecy throughput across devices through simultaneous optimization of the RIS's phase shift matrices and time allocations for both downlink and uplink phases. In a related study, Zheng et al. harnessed the capabilities of RIS to boost both energy and spectral efficiencies within cooperative WPCNs [20]. Their methodology, centered on IRS-facilitated cooperation, resulted in a notable throughput enhancement of 91.85% compared to scenarios lacking IRS support. Differently, Hameed et al. integrated a passive RIS within a cognitive radio (CR)-enhanced WPCN framework, assessing the influence of the RIS on aggregate throughput for cognitive users, especially in environments potentially populated by primary users [25].

Recent research has addressed the limitations of systems using a single RIS by implementing advanced strategies. These strategies include deploying multiple RISs, fostering RIS cooperation, applying dynamic control, and utilizing hybrid beamforming to fully exploit RIS technology in enhancing wireless communication [28–35]. A multi-RIS configuration involves placing RISs near both the H-AP and wireless devices, significantly improving communication efficiency. This arrangement introduces additional flexibility through a dual-reflection path involving each RIS, offering extra advantages, particularly when direct and single-reflection paths are obstructed [28]. Han et al. proposed a co-

operative double-IRS-aided MIMO system to boost signal coverage and communication performance, focusing on capacity maximization by jointly optimizing transmit and passive beamforming matrices. This work introduces a low-complexity algorithm and, through extensive numerical analysis, shows that the system substantially outperforms conventional single-IRS setups by leveraging cooperative power and spatial multiplexing gains [31]. Nhu et al. introduced and analyzed two multi-RIS-aided wireless system schemes, the exhaustive RIS-aided (ERA) and opportunistic RIS-aided (ORA), using statistical models for end-to-end channel characterization. Their findings reveal that the ERA scheme outperforms the ORA in terms of outage probability and ergodic capacity, underscoring the significant impact of RIS configurations and placements under independently non-identically distributed fading channels on system performance [33]. Hou et al. presented a distributed RISs framework (DRF) to improve 6G wireless communication in the THz domain, demonstrating through simulations how distributed RISs effectively mitigate human blockage, enhance THz signal coverage, and improve signal-to-noise ratios (SNRs) and quality of service (QoS), thereby establishing a foundation for efficient THz internet of things (IoT) networks [34]. Li et al. explored the coverage probability in a 3D downlink millimeter-wave network assisted by RIS, emphasizing the influence of the number of RISs and unit cells per RIS on network performance in the presence of blockages. The results indicate that densely deployed small-scale RISs more effectively enhance coverage in areas with dense blockages or short distances, while sparsely deployed large-scale RISs are more suitable for environments with sparse blockages or longer transmission distances [35].

However, deployments involving passive RISs, despite their pronounced advantages, encounter specific limitations. These limitations are coherent with theoretical insights suggesting optimal placement of a RIS proximal to either the H-AP or the devices to mitigate the channel gain attenuation across the communication channels connecting the RIS with both the H-AP and end devices [16]. Consequently, passive-RIS configurations may face challenges such as limited transmission range, critical obstruction issues, diminished passive beam gains, and constrained multiplexing gains due to channel correlations. These factors underscore the imperative for continued research and the development of innovative deployment tactics to fully leverage RIS's potential in enhancing communication performance.

1.2.2. Active RIS-Aided Networks

Despite the potential of passive reconfigurable intelligent surfaces (RIS) in enhancing wireless communications, they encounter a particular challenge referred to as *double-fading attenuation*. This occurs because reflected signals must go through multiple links, reducing their strength and limiting the coverage area of each RIS [36]. One approach to mitigating this issue aims to increase the number of elements on the RIS. On the other hand, this can be technically complex and expensive, involving hardware design and implementation. This may not always be practical in real-world scenarios. Another option is to position the RIS closer to the H-AP or end devices. This reduces the range of signals that travel through the multiple links, which helps improve the signal strength and coverage. Nevertheless, adjusting the proximity of the RIS also comes with practical challenges [37]. In light of these complexities, researchers are exploring active RIS technology as an alternative solution [38–46]. In contrast to passive RIS, active RIS have the ability to not only reflect signals but also actively boost them. This attribute provides a more effective solution to mitigate signal degradation without necessitating a large array of reflectors. This innovation presents a promising avenue for markedly improving the practicality and efficiency of wireless communications, potentially leading to enhanced network throughput and broader coverage. Zhang et al. have documented that active RIS can furnish a substantial increase in sum-rate performance by 130% within a standard wireless framework, a considerable improvement over the 22% gain offered by passive RIS, thereby addressing the challenge of multiplying channel gain attenuation [38]. Furthermore, Zeng et al. investigated the

deployment of an active RIS in a WPCN, leveraging its advantages to optimize the weighted sum throughput, thereby ensuring equitable throughput distribution [40].

The evaluation of an active RIS-enhanced WPCN aimed to harness the advantages offered by active RIS technology. Incorporating active RIS into WPCNs introduces significant benefits, yet it also presents novel challenges. The simultaneous optimization of resources, like time allocation, along with the tuning of active RIS components, grows in complexity due to the presence of both WET and WIT within WPCNs. Active RIS, with its capability for signal amplification, adds further complexity to the optimization task by introducing more variables and constraints, particularly with the need to manage the amplified thermal noise that impacts both downlink and uplink transmissions. Achieving stability between enhancing signal strength and reducing noise on the uplink adds further complexity. Overcoming these challenges necessitates innovative and sophisticated approaches to fully exploit active RIS technology for WPCN performance enhancement. This entails navigating the complexities associated with integrating and efficiently operating active RIS components in the network. The primary contributions of this work are outlined as follows.

- The study compares active and passive reconfigurable intelligent surfaces (RIS) to optimize the total throughput in wireless-powered communication networks (WPCNs). We introduce an approach involving active RIS to enhance WPCN performance. An optimization problem was formulated to maximize the total throughput of wireless devices within the WPCN. This entailed optimizing the amplification coefficients, phase shift matrices of RIS elements, and time allocations for both downlink and uplink while ensuring that the minimum energy requirements of wireless devices were met.
- We exploited an approach based on alternating optimization (AO) to tackle the non-linear total throughput optimization challenge. By dividing the complex maximization problem into smaller, manageable sub-problems and addressing them in a sequential manner, we were able to iteratively find a near-optimal configuration for the RIS components, considering specific time allocations. We utilized successive convex approximation (SCA) methods to reformulate the original non-convex problem into a set of convex sub-problems, which were then resolved through iterative processes. Additionally, we employed a feasible point pursuit strategy to identify an initial viable point, thereby accelerating the algorithm's convergence rate.
- The study used numerical simulations to assess the proposed methodologies. The performance evaluation showed that the active RIS-assisted WPCN significantly outperformed a network assisted by passive RIS. This highlights the substantial impact and superior performance of using active RIS in enhancing the efficiency of WPCNs. Important notations and their definitions are in Table 1.

Table 1. Notations.

Symbol	Definitions
$x \in A$	x is the element in set A
$ a $	The absolute value of a complex-valued scalar a
$\ \mathbf{a}\ $	The norm of a complex-valued vector \mathbf{a}
$[\mathbf{A}]_{a,b}$	The element in matrix \mathbf{A} positioned at a_{th} row and b_{th} column
$\text{diag}(\mathbf{a})$	The diagonal matrix of vector \mathbf{a}
$\text{rank}(\mathbf{A})$	The rank of matrix \mathbf{A}
$(\mathbf{a})^H$	The conjugate transpose of a complex-valued vector \mathbf{a}
$\mathbf{A} \succeq 0$	Positive semidefinite matrix \mathbf{A}
j	The imaginary unit, i.e., $j^2 = -1$
$\mathbb{C}^{a \times b}$	The space of $a \times b$ complex-valued matrices

2. Active RIS-Aided WPCN

2.1. System Model

This section introduces a WPCN assisted by an active RIS, as depicted in Figure 1. The network comprises an H-AP with a single antenna, an RIS featuring M active reflective elements, and N single-antenna wireless devices, labeled as WD_1, WD_2, \dots, WD_N . An active RIS is comprised of a smart controller and designed reflecting elements, adjusted by the controller via FPGA-based control. Each element reflects signals with a customized phase and amplitude based on electromagnetic principles. The flat-fading channel gains from H-AP to RIS; from RIS to the n_{th} , the users are showing as $\mathbf{g} \in \mathbb{C}^{M \times 1}$ and $\mathbf{h}_n \in \mathbb{C}^{M \times 1}$, respectively. Obstacles block the direct path between the H-AP and the devices, necessitating the use of reflective elements to aid in the transmission of wireless energy and information. Conversely, the algorithm designed can also accommodate scenarios where direct connections exist between the transmitter and the receiver. The channels for downlink communication enable the WET from the H-AP to the devices, whereas the uplink are responsible for WIT from the devices back to the H-AP. The communication links are modeled as quasi-static, exhibiting flat fading properties that stay uniform throughout a coherence period marked by T . On the other hand, these channel characteristics may vary between different coherence intervals. Despite this variability, the transmitter is assumed to possess immediate access to the current channel state information at the initiation of each coherence interval. For simplicity, the convention of setting $T = 1$ was adopted throughout this paper.

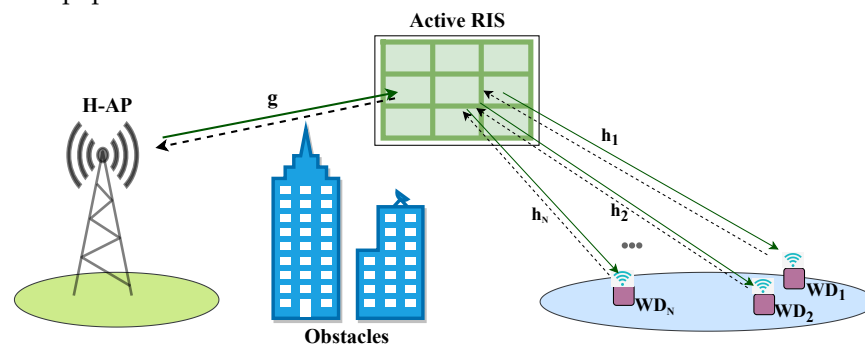


Figure 1. Active RIS-assisted energy and information transmission network.

The coherence period is segmented into two distinct phases, as depicted in Figure 2. In the initial phase, identified by the time slot τ , the end devices harvest energy from the signal transmitted by the H-AP. These devices do not have a power supply battery and rely entirely on the energy for their subsequent uplink communication tasks. In the subsequent phase, using the remaining time $(1 - \tau)$, all devices simultaneously send their information signals to the H-AP.

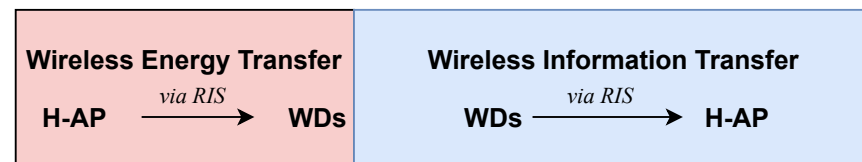


Figure 2. Time division duplex frame-based transmission scheme.

2.1.1. Energy Transmission

In the first phase, n_{th} device received the energy signal sent by H-AP is

$$y_n = \sqrt{P_A} (\mathbf{h}_n^H \Phi_d \mathbf{g}) x_0 + \mathbf{h}_n^H \Phi_d \mathbf{z}_I + z_n, \quad \forall n \tag{1}$$

Here, x_0 , $E[|x_0|^2] = 1$, is the energy signal sent by H-AP in the downlink transmission; P_A is the transmission power available at the H-AP; $\Phi_d = \text{diag}(a_1, a_2, \dots, a_M) \text{diag}(e^{j\theta_1}, e^{j\theta_2}, \dots, e^{j\theta_M})$, is the active-RIS reflection matrix. In this matrix, a_m and θ_m correspond to the amplification factor and phase shift of the m_{th} reflecting element, respectively ($m = 1, 2, 3, \dots, M$). Specifically, $\mathbf{z}_I \sim \mathcal{CN}(0, \sigma_I^2)$ and $z_n \sim \mathcal{CN}(0, \sigma_n^2)$ denote the amplification noise at each element of the RIS and the additive noise at the WD_n , respectively. In practical contexts, the receiver noise had a negligible impact on the energy-receiving nodes. Consequently, z_n can be disregarded safely within further problem formulations. Unlike the noise-free scenario seen with passive RIS, amplification noise for IRS elements cannot be overlooked in this case.

Therefore, the amount of energy harvested at the n_{th} device during the downlink interval τ , denoted by E_n , is expressed as

$$E_n = \zeta_n \tau \left(P_A |\mathbf{h}_n^H \Phi_d \mathbf{g}|^2 + \sigma_I^2 \|\mathbf{h}_n^H \Phi_d\|^2 \right), \quad \forall n \tag{2}$$

where $0 < \zeta_n < 1$ is the energy harvesting efficiency at the n_{th} device.

2.1.2. Information Transmission

During information transmission on the uplink, the H-AP employs NOMA, using successive interference cancellation (SIC) to mitigate multi-user interference. In particular, the H-AP initiates the process by decoding the information signals of all devices denoted by k , where $k < n$, to decode the information signal of the n_{th} wireless device. Subsequently, the decoded signals corresponding to these k_{th} users are sequentially subtracted from the received signal, following the order of $k = 1, 2, \dots, n - 1$, effectively eliminating interference [47].

The signal received from a user indexed as k , with $k > n$, is treated as noise. Consequently, the attainable throughput of the n_{th} user, measured in bits per second per Hertz (bps/Hz), can be expressed as follows:

$$r_n(\tau, p_n, \Phi_u) = (1 - \tau) \log_2 \left[1 + \frac{p_n |\mathbf{g}^H \Phi_u \mathbf{h}_n|^2}{\sum_{k=n+1}^K p_k |\mathbf{g}^H \Phi_u \mathbf{h}_k|^2 + \sigma_I^2 \|\mathbf{g}^H \Phi_u\|^2 + \sigma_a^2} \right], \quad \forall n \tag{3}$$

$\Phi_u = \text{diag}(b_1, b_2, \dots, b_M) \text{diag}(e^{j\omega_1}, e^{j\omega_2}, \dots, e^{j\omega_M})$ is the active-RIS reflection matrix for uplink with b_m and ω_m ; for $m = 1, 2, 3, \dots, M$, are the amplification factor and phase shifts of the m_{th} reflecting elements. p_n is the harvested power of WD_n , and σ_a^2 is the noise variance at the H-AP.

Therefore, the achievable total throughput in the $1 - \tau$ interval for the n_{th} device is given by [48,49].

$$R(\tau, p_n, \Phi_u) = \sum_{n=1}^N (1 - \tau) \log_2 \left[1 + \frac{p_n |\mathbf{g}^H \Phi_u \mathbf{h}_n|^2}{\sum_{k=n+1}^K p_k |\mathbf{g}^H \Phi_u \mathbf{h}_k|^2 + \sigma_I^2 \|\mathbf{g}^H \Phi_u\|^2 + \sigma_1^2} \right] \tag{4a}$$

$$R(\tau, \Phi_d, \Phi_u) = (1 - \tau) \log_2 \left[1 + \frac{\sum_{n=1}^N \zeta_n \frac{\tau}{1-\tau} \left(P_A |\mathbf{h}_n^H \Phi_d \mathbf{g}|^2 + \sigma_I^2 \|\mathbf{h}_n^H \Phi_d\|^2 \right) |\mathbf{g}^H \Phi_u \mathbf{h}_n|^2}{\sigma_I^2 \|\mathbf{g}^H \Phi_u\|^2 + \sigma_a^2} \right] \tag{4b}$$

2.2. Sum Throughput Maximization Problem

The objective of this study was to enhance the aggregate throughput of wireless devices by efficiently leveraging available resources in an active RIS-assisted WPCN. Equation (4) shows that the time allocation for uplink and downlink transmissions and the active RIS configuration directly influenced the total throughput. When downlink time allocation is increased, the harvested energy increases, diminishing the time available for end devices to transmit information, ultimately reducing network throughput. On the other hand, decreasing the downlink time allocation would offer more time for information transmission but at the expense of harvested energy. Therefore, finding the optimal balance between the downlink and uplink time allocation becomes imperative to maximize throughput. In contrast to passive RIS, the design of active RIS increases complexity because of the need to optimize the amplitude coefficients. This optimization process considers the total power budget allocated for IRS elements. Similarly, the RIS reflecting elements can be manipulated, aligning their beams constructively in the intended direction. This adjustment has the potential to enhance network performance significantly.

The main goal was maximizing the overall throughput by jointly optimization and involving both time allocation and the configuration of active RIS matrices. This approach seeks to achieve the utmost efficiency in utilizing the available resources. The optimization problem is expressed as follows:

$$\max_{\tau, \Phi_d, \Phi_u} R(\tau, \Phi_d, \Phi_u) \quad (5a)$$

$$\text{s.t. } \zeta_n \tau \left(P_A \left| \mathbf{h}_n^H \Phi_d \mathbf{g} \right|^2 + \sigma_I^2 \|\mathbf{h}_n^H \Phi_d\|^2 \right) \geq e_{min}, \quad \forall_n \quad (5b)$$

$$P_A \|\mathbf{g}^H \Phi_d\|^2 + \sigma_I^2 \|\Phi_d\|^2 \leq P_I \quad (5c)$$

$$p_n \|\mathbf{h}_n^H \Phi_u\|^2 + \sigma_I^2 \|\Phi_u\|^2 \leq P_I, \quad \forall_n \quad (5d)$$

$$a_m \leq a_{max}, \quad m = 1, 2, 3, \dots, M \quad (5e)$$

$$b_m \leq b_{max}, \quad m = 1, 2, 3, \dots, M, \quad (5f)$$

$$0 \leq \tau \leq 1 \quad (5g)$$

In Problem (5), the optimization maximizes the total throughput among all N devices. Constraint (5b) aims to ensure the minimum harvesting energy requirement on the downlink. On the other hand, unlike passive RIS scenarios, active RIS introduces additional constraints denoted as (5c)–(5f). These constraints address amplification power considerations. In particular, (5c) and (5d) pertain to amplification power limitations, where P_I is the available total power in the active IRS for amplification. Constraints (5e) and (5f) establish a power amplification restriction. Within the active IRS framework, it is possible to allocate the available power for amplification to enhance the incident signals through active loads, albeit after accounting for power consumption associated with hardware. Nevertheless, the amplification of incident signals is capped at predetermined maximum amplitudes, denoted as a_{max} and b_{max} for the downlink and uplink, respectively.

Constraint (5g) introduces the total time constraint governing the downlink and uplink phases. Solving Problem (5) analytically is notably complex owing to the intricate nature of the non-convex objective function and the interconnected constraints on optimal variables. As a result, an alternating optimization method was used to solve the maximization problem. This approach overcomes the challenges associated with the complexity and interdependencies of the problem.

3. AO-SCA-Based Algorithm

The sum-throughput optimization Problem (5) is notably intricate and challenging to address due to the interdependence of variables and the non-linear nature of both the objective functions and constraints. To tackle Problem (5), the approach involved breaking it down into two more manageable sub-problems, which were then addressed through

iterative solutions. Initially, the focus was on stabilizing the uplink beamforming vector, which allowed for the optimization of RIS matrices on the downlink. Subsequently, with the downlink beamforming parameters set, attention was turned to optimizing the uplink beamforming, thus achieving a near-optimal solution for this component as well.

3.1. Optimize the Downlink RIS Matrix by Fixing the Uplink RIS Matrix

In this step, the uplink RIS matrix and time allocations were first fixed to optimize the downlink RIS vectors for phase and amplitude coefficients. We defined $\mathbf{v}_d = [a_1 e^{j\theta_1}, a_2 e^{j\theta_2}, \dots, a_M e^{j\theta_M}]$ and $\mathbf{h}_{en} = \text{diag}(\mathbf{g})\mathbf{h}_n$. Problem (5) was then reduced into the following maximization of sum-harvested power problem by fixing τ and Φ_u and omitting unnecessary constant terms in the objective function.

$$\max_{\mathbf{v}_d} \sum_{n=1}^N \zeta_n \frac{\tau}{1-\tau} \left(P_A |\mathbf{h}_{en}^H \mathbf{v}_d|^2 + \sigma_I^2 \|\mathbf{h}_{en}^H \mathbf{v}_d\|^2 \right) \quad (6a)$$

$$\text{s.t.} \quad (5b), (5c), (5d), \text{ and } (5e) \quad (6b)$$

A concave lower bound needs to be found for these terms because terms $|\mathbf{h}_{en}^H \mathbf{v}_d|^2$ and $\|\mathbf{h}_n^H \mathbf{v}_d\|^2$ in (5b) are convex with respect to \mathbf{v}_d . Let $\mathbf{v}_d^{(i)}$ be the value of \mathbf{v}_d in the i_{th} iteration of successive convex approximation process. Therefore, this lower bound was obtained using the first-order Taylor underestimation as follows:

$$\begin{aligned} |\mathbf{h}_{en}^H \mathbf{v}_d|^2 &\geq 2\mathcal{R}(\mathbf{v}_d^{(i)H} \mathbf{h}_{en} \mathbf{h}_{en}^H \mathbf{v}_d) - |\mathbf{h}_{en}^H \mathbf{v}_d^{(i)}|^2 \\ &\triangleq f_{en}(\mathbf{v}_d, \mathbf{v}_d^{(i)}) \end{aligned} \quad (7)$$

Hence by applying (7), we can rewrite Problem (6) in equivalent form as follows:

$$\max_{\mathbf{v}_d} \sum_{n=1}^N \zeta_n \frac{\tau}{1-\tau} \left(P_A |\mathbf{h}_{en}^H \mathbf{v}_d|^2 + \sigma_I^2 \|\mathbf{h}_n^H \mathbf{v}_d\|^2 \right) \quad (8a)$$

$$\text{s.t.} \quad 0 \geq \frac{e_{min}}{\zeta_n \tau} - \left(P_A f_{en}(\mathbf{v}_d, \mathbf{v}_d^{(i)}) + \sigma_I^2 f_n(\mathbf{v}_d, \mathbf{v}_d^{(i)}) \right), \quad \forall_n \quad (8b)$$

$$0 \geq P_A |\mathbf{g}^H \mathbf{v}_d|^2 + \sigma_I^2 \|\mathbf{v}_d\|^2 - P_I \quad (8c)$$

$$0 \geq A_n \left(P_A |\mathbf{h}_{en}^H \mathbf{v}_d|^2 + \sigma_I^2 \|\mathbf{h}_n^H \mathbf{v}_d\|^2 \right) - P_I, \quad \forall_n \quad (8d)$$

$$0 \geq a_m - a_{max}, \quad m = 1, 2, 3, \dots, M \quad (8e)$$

where $A_n = \zeta_n \frac{\tau}{1-\tau} (\|\mathbf{h}_n^H \Phi_u\|^2 + \sigma_I^2 \|\Phi_u\|^2)$. Hence, Problem (8) is convex and can be easily solved by CVX.

Initialization

A feasible starting point for Problem (8) can be identified. The SCA technique achieves convergence when initiated from a feasible point. Given its iterative nature, the SCA method may require extensive computation time if the initial variables are not aptly chosen. To ensure rapid convergence of the SCA algorithm, a feasible point was derived using a feasible point pursuit strategy. In this context, slack variables $\mathbf{s}_1 = [s_{1,1}, s_{1,2}, \dots, s_{1,N}]$, \mathbf{s}_2 , $\mathbf{s}_3 = [s_{3,1}, s_{3,2}, \dots, s_{3,N}]$, and $\mathbf{s}_4 = [s_{4,1}, s_{4,2}, \dots, s_{4,M}]$ were introduced to facilitate the determination of a feasible starting point for the subsequent problem formulation.

$$\max_{\mathbf{v}_d, \mathbf{s}_1, \mathbf{s}_2, \mathbf{s}_3, \mathbf{s}_4} \sum_{n=1}^N s_{1,n}^{(i)} + s_2^{(i)} + \sum_{n=1}^N s_{3,n}^{(i)} + \sum_{m=1}^M s_{4,m}^{(i)} \quad (9a)$$

$$\text{s.t. } 0 \geq \frac{e_{\min}}{\zeta_n \tau} - \left(P_A f_{en}(\mathbf{v}_d, \mathbf{v}_d^{(i)}) + \sigma_I^2 f_n(\mathbf{v}_d, \mathbf{v}_d^{(i)}) \right) - s_{1,n}^{(i)}, \quad \forall_n \quad (9b)$$

$$0 \geq P_A \left| \mathbf{g}^H \mathbf{v}_d \right|^2 + \sigma_I^2 \|\mathbf{v}_d\|^2 - P_I - s_2^{(i)} \quad (9c)$$

$$0 \geq A_n \left(P_A \left| \mathbf{h}_{en}^H \mathbf{v}_d \right|^2 + \sigma_I^2 \|\mathbf{h}_n^H \mathbf{v}_d\|^2 \right) - P_I - s_{3,n}^{(i)}, \quad \forall_n \quad (9d)$$

$$0 \geq a_m - a_{\max} - s_{4,m}^{(i)}, \quad m = 1, 2, 3, \dots, M \quad (9e)$$

Hence, the non-convex issue presented in Problem (6) can be transformed into an iterative convex problem, as outlined in Problem (9). At each iteration, the solution to Problem (9), represented by $[\mathbf{v}_d^{(i)}, \mathbf{s}_1^{(i)}, s_2^{(i)}, \mathbf{s}_3^{(i)}, \mathbf{s}_4^{(i)}]$, serves as a feasible point for the i_{th} iteration.

3.2. Optimize the Uplink RIS Matrix by Fixing the Downlink RIS Matrix

Next, the amplitude and phase shift vectors for the uplink were optimized by fixing the downlink RIS matrix and time allocation. Moreover, $\mathbf{v}_u = [b_1 e^{j\omega_1}, b_2 e^{j\omega_2}, \dots, b_M e^{j\omega_M}]$ and Problem (5) is reformulated into the following sub-problem.

$$\max_{\mathbf{v}_u} (1 - \tau) \log_2 \left[1 + \frac{\sum_{n=1}^N p_n \left| \mathbf{h}_{en}^H \mathbf{v}_u \right|^2}{\sigma_I^2 \|\mathbf{g}^H \Phi_u\|^2 + \sigma_a^2} \right] \quad (10a)$$

$$\text{s.t. } (5d), \text{ and } (5f) \quad (10b)$$

An auxiliary variable $\gamma \geq \frac{\sum_{n=1}^N p_n \left| \mathbf{h}_{en}^H \mathbf{v}_u \right|^2}{\sigma_I^2 \|\mathbf{g}^H \Phi_u\|^2 + \sigma_a^2}$ is introduced because of the non-convexity of the objective function, and Problem (10) is rewritten as

$$\max_{\gamma, \mathbf{v}_u} (1 - \tau) \log_2 [1 + \gamma] \quad (11a)$$

$$\text{s.t. } 0 \geq p_n \frac{\left| \mathbf{h}_{en}^H \mathbf{v}_u \right|^2}{\gamma} - \sigma_I^2 f_g(\mathbf{v}_u, \mathbf{v}_u^{(i)}) - \sigma_a^2 \quad (11b)$$

$$0 \geq p_n \left| \mathbf{h}_n^H \mathbf{v}_u \right|^2 + \sigma_I^2 \|\mathbf{v}_u\|^2 - P_I \quad (11c)$$

$$0 \geq b_m - b_{\max}, \quad m = 1, 2, 3, \dots, M \quad (11d)$$

where $f_g(\mathbf{v}_u, \mathbf{v}_u^{(i)}) \triangleq 2\mathcal{R}(\mathbf{v}_u^{(i)H} \mathbf{g} \mathbf{g}^H \mathbf{v}_u) - \left| \mathbf{g}^H \mathbf{v}_u^{(i)} \right|^2$ defines the concave lower bound of $\left| \mathbf{g}^H \mathbf{v}_u \right|^2$ and $\mathbf{v}_u^{(i)}$ shows the uplink vector solution in i_{th} iteration. Similarly, as in Problem (9), the initial feasible point of Problem (11) can be found.

Problem (8) and Problem (11) are solved successively until the convergence meets and the sub-optimal point is reached for $[\mathbf{v}_d^{(*)}, \mathbf{v}_u^{(*)}]$. Next, a 1-D exhaustive search is used to find the optimal value of τ for the given $[\mathbf{v}_d^{(*)}, \mathbf{v}_u^{(*)}]$. The proposed AO-SCA-based solution is summarized in Algorithm 1.

Algorithm 1 The proposed AO-SCA-based algorithm to find solution to Problem (5)

```

1: Set the initial values for  $\tau, \mathbf{v}_d, \mathbf{v}_u$ , tolerance value  $\zeta$ 
2: // main loop:
3: repeat
4:   Search the initial feasible point for  $[\mathbf{v}_d^{(0)}, \mathbf{s}_1^{(0)}, s_2^{(0)}, \mathbf{s}_3^{(0)}, \mathbf{s}_4^{(0)}]$  by solving Problem (9)
   using CVX solver and find  $q^{(0)} = \frac{\sum_{n=1}^N \zeta_n \frac{\tau}{1-\tau} \left( P_A \left| \mathbf{h}_{en}^H \mathbf{v}_d^{(0)} \right|^2 + \sigma_I^2 \|\mathbf{h}_n^H \mathbf{v}_d^{(0)}\|^2 \right) - \left( \sum_{n=1}^N s_{1,n}^{(0)} + s_2^{(0)} + \sum_{n=1}^N s_{3,n}^{(0)} + \sum_{m=1}^M s_{4,m}^{(0)} \right)}$ 
5:   // initial loop:
6:    $i = 0$ 
7:   repeat
8:     Solve Problem (8) using MATLAB CVX solver and compute
      $[\mathbf{v}_d^{(i)*}, \mathbf{s}_1^{(i)*}, s_2^{(i)*}, \mathbf{s}_3^{(i)*}, \mathbf{s}_4^{(i)*}]$ 
9:      $i = i + 1$ 
10:    Assign  $\mathbf{v}_d^{(i)} \leftarrow \mathbf{v}_d^{(i-1)*}, \mathbf{s}_1^{(i)} \leftarrow \mathbf{s}_1^{(i-1)*}, s_2^{(i)} \leftarrow s_2^{(i-1)*}, \mathbf{s}_3^{(i)} \leftarrow \mathbf{s}_3^{(i-1)*}, \mathbf{s}_4^{(i)} \leftarrow \mathbf{s}_4^{(i-1)*}$ 
11:    Compute  $q^{(i)} = \frac{\sum_{n=1}^N \zeta_n \frac{\tau}{1-\tau} \left( P_A \left| \mathbf{h}_{en}^H \mathbf{v}_d^{(i)} \right|^2 + \sigma_I^2 \|\mathbf{h}_n^H \mathbf{v}_d^{(i)}\|^2 \right) - \left( \sum_{n=1}^N s_{1,n}^{(i)} + s_2^{(i)} + \sum_{n=1}^N s_{3,n}^{(i)} + \sum_{m=1}^M s_{4,m}^{(i)} \right)}$ 
12:    until
13:     $\frac{|q^{(i)} - q^{(i-1)}|}{q^{(i-1)}} \leq \zeta$ 
14:    // main loop:
15:    Assign  $\mathbf{v}_d^* \leftarrow \mathbf{v}_d^{(i)}$ 
16:    Next
17:    Set the value for  $\mathbf{v}_d = \mathbf{v}_d^*$ 
18:    Solve Problem (11) as similar to step 4–15 and get  $\mathbf{v}_u^*$ 
19:    until convergence achieved
20:    output  $\mathbf{v}_d^*, \mathbf{v}_u^*$ 
21: Do exhaustive search to find  $\tau^*$ 

```

3.3. Complexity Analysis

This study examined the computational complexity of Algorithm 1. Problem (5) was solved using a convex optimization solver based on the interior-point method.

The complexity of the Algorithm 1 is $\mathcal{O}\left(I_{AO}(I_A + I_B)[(2M + 2N + 1)^{3.5} \log(1/\epsilon)] + K\right)$, where I_A and I_B are the iterations of the SCA method for solving the uplink and downlink RIS matrices; I_{AO} is the average number of iterations of the main loop of AO to make the Algorithm 1 to converge. On the other hand, K presents the search space for an exhaustive search of the optimal time allocation and ϵ is the preset solution accuracy.

4. Comparative Analysis and Discussions

In this section, the comparative analysis of active RIS-assisted networks was compared with the other passive networks, and a detailed discussion of the numerical results is provided. In the simulation setup, this study considered a three-dimensional coordinate system, where the H-AP and the IRS are located at $(0m, 0m, 0m)$ and $(2m, 0m, 2m)$, respectively. On the other hand, the wireless devices are distributed randomly and uniformly within a radius of $2m$ centered at $(2m, 0m, 0m)$. The maximum power budget was set for the H-AP and active RIS, i.e., $P_A = P_I = 30$ dBm, the receiver energy-harvesting efficiency at $\zeta_n = \zeta = 0.8$, and noise variance for H-AP and active RIS elements, $\sigma_a^2 = \sigma_I^2 = -70$ dBm. In the simulation setup, we modeled the distance-dependent path loss as $\rho_n = A_0 \frac{d^{-\alpha}}{d_0}$, where $A_0 = -30$ dBm is the free space path loss at the reference distance of $d_0 = 1m$; and α is the path loss component, which is set to 2 and 2.2 for H-AP to RIS and RIS to users,

respectively. Obstacles block the direct channels from the H-AP to users, necessitating the support of RIS for wireless communication. The reflection links through the RIS are characterized by Rician fading, expressed as

$$\mathbf{g} = \sqrt{\frac{\kappa}{1+\kappa}} \mathbf{g}^{LOS} + \sqrt{\frac{1}{1+\kappa}} \mathbf{g}^{NLOS}, \tag{12}$$

where κ represents the Rician factor, set at 3. Here, \mathbf{g}^{NLOS} symbolizes the non-line-of-sight components, adhering to standard Rayleigh fading with zero mean and unity variance, and \mathbf{g}^{LOS} is the line-of-sight component. The LOS component can be described using a far-field uniform linear array (ULA) formulation as $\mathbf{g}^{LOS} = [1, e^{-j2\pi \frac{s}{\lambda} \sin(\theta)}, \dots, e^{-j2\pi \frac{s}{\lambda} (M-1) \sin(\theta)}]^T$, where s denotes the distance between elements of the RIS (assumed to be half the wavelength $\lambda/2$), and θ is the angle related to either the angle-of-departure (AOD) or angle-of-arrival (AOA) at the RIS elements.

Figure 3 presents the convergence behavior of the proposed solution. In particular, it depicts the sum throughput maximization function for different numbers of IRS elements. The proposed algorithm demonstrates remarkably fast convergence. This rapid convergence can be attributed to the careful initialization procedure, which leverages an initial pursuit method to set the initial variable values. This strategic initialization method improves the subsequent optimization process, facilitating the efficiency of the algorithm in reaching convergence.

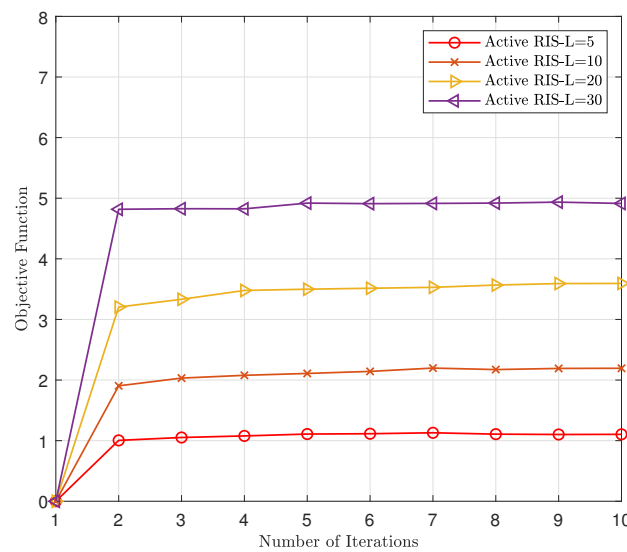


Figure 3. Convergence of the proposed A0-SCA-based algorithm.

Figure 4 presents the relationship between the total throughput and the number of RIS elements. The achievable throughput increased as the number of RIS elements increased. Two scenarios were compared for further analysis: one employing an active RIS-based WPCN and the other utilizing a passive RIS-based WPCN. In both scenarios, two different time allocation strategies were considered: optimal and equal division between the downlink and uplink phases. A substantial increase in throughput was observed using an active RIS instead of a passive one. Furthermore, the figure depicts the importance of optimizing time allocation rather than employing an equal division strategy because it enhances the overall throughput significantly. Hence, strategic time allocation plays a critical role in maximizing the efficiency and performance of the communication network.

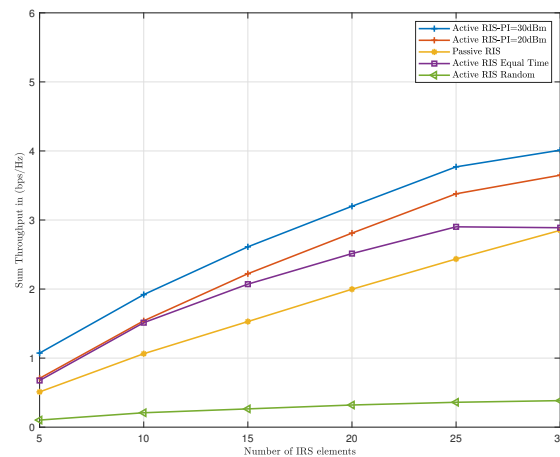


Figure 4. Sum throughput in bps/Hz versus the number of IRS elements.

This study examined the relationship between the total available power at the H-AP and its impact on the overall total throughput in this system (Figure 5). Each wireless node could harvest more energy when the transmit power was increased. This surplus energy increased the power available for transmitting information in the uplink. Consequently, the increased power resources led to higher throughput levels because more energy was allocated to the data transmission process. On the other hand, the active RIS elements may impose a maximum threshold on the amplitude, which is influenced by the practical limitations associated with RIS elements. Active RIS elements provide greater flexibility in managing power allocation and signal amplification, leading to improved overall system performance.

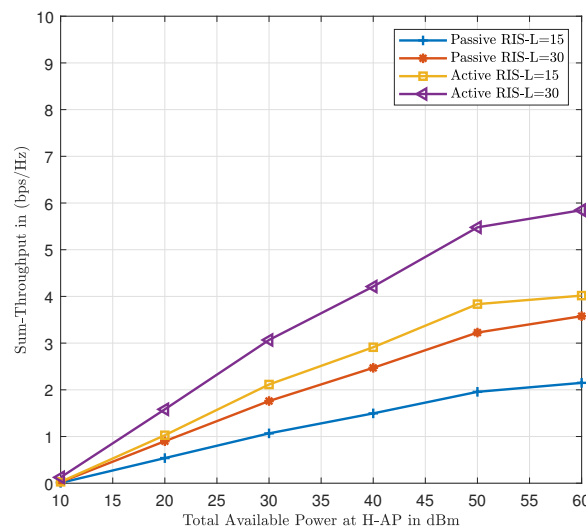


Figure 5. Sum throughput in bps/Hz versus transmit power available at H-AP.

Figure 6 shows a detailed analysis of the throughput as it relates to the maximum amplitude constraint, α_{max} , of the signal incident on the active RIS. It is predicated on the assumption that the amplitude constraints for both downlink and uplink phases are identical, denoted as $a_{max} = b_{max} = \alpha_{max}$. The findings distinctly demonstrate an increase in total throughput with a rise in α_{max} , a phenomenon credited to the active RIS’s capability to deliver enhanced amplification gain. This effectively counters signal degradation and boosts the signal strength received by the devices.

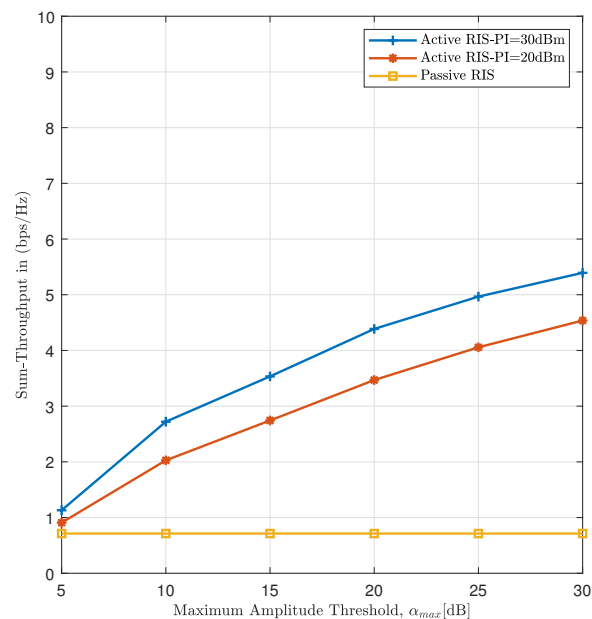


Figure 6. Sum throughput versus the increasing maximum amplitude limit.

4.1. Discussion on Practical Applicability of Active RIS in WPCNs

This study has demonstrated the theoretical advantages of employing active RIS in WPCNs to maximize network throughput. While our results offer promising insights into the potential of active RIS, translating these theoretical findings into practical applications necessitates addressing several challenges and considerations.

4.1.1. Computational Efficiency

In Section 3.3, we conducted a comprehensive complexity analysis of the proposed AO-SCA algorithm, thoroughly quantifying the computational resources required. Furthermore, Figure 3 in our document illustrates the algorithm's fast convergence, demonstrating the practical viability of our method. This rapid convergence is attributed to the feasible point pursuit method used for algorithm initialization, which significantly reduces computational effort by providing an efficient starting point. This approach addresses computational load concerns and operational latency, making our algorithm suitable for dynamic environments where quick adaptation is critical.

However, future research should investigate algorithmic optimizations to reduce computational requirements without sacrificing performance. In this context, exploring artificial intelligence (AI)-based algorithms, particularly reinforcement learning (RL), offers a promising direction for future work. RL's model-free optimization capabilities, capable of dynamically adapting to changing network conditions, make it ideal for complex, dynamic systems where traditional optimization methods may be inadequate. Investigating RL could yield innovative, data-driven strategies for managing RIS-aided WPCNs, potentially revealing new avenues for throughput maximization and energy efficiency improvement. Additionally, the implementation of distributed computing techniques could lighten the processing load on individual network nodes, enhancing the system's scalability and efficiency.

4.1.2. Deployment Challenges

Integrating active RIS into existing network infrastructures introduces several deployment challenges, such as power supply requirements for active components and ensuring compatibility with prevailing communication standards. To tackle these challenges, we incorporate constraints (5c)–(5f) in Problem (5), focusing on amplification power and

amplitude limitations within the active RIS framework. Constraints (5c) and (5d) specifically address the limitations on power available for signal amplification by the active RIS. Furthermore, constraints (5e) and (5f) establish the boundaries for power amplification, permitting the distribution of available amplification power to enhance incoming signals through active loads while factoring in the power consumption of the hardware components. Nonetheless, the signal enhancement via amplification is restricted to predetermined maximum amplitudes for the downlink and uplink phases, respectively. Integrating these constraints into the optimization problem offers critical insights for designing efficient and robust WPCNs that demonstrate the practical application of active RISs in enhancing network efficiency. Future research could focus on designing energy-efficient active RIS units and developing adaptable interface modules to ensure smooth integration with diverse network architectures.

5. Conclusions

This paper conducted a comparative analysis of active RISs and passive RISs, specifically focusing on optimizing resource allocation in RIS-assisted wireless-powered communication networks (WPCNs). The objective was to maximize the total throughput of the network by harnessing the active capabilities of RISs. In conclusion, RISs are a promising technology to enhance wireless networks by intelligently manipulating electromagnetic waves, improving signal quality, and mitigating interference. Passive RISs offer an energy-efficient solution but may have limitations in coverage and spatial gain. Active RIS technology has been introduced to address these limitations, which reflect signals and actively amplify them, potentially overcoming challenges such as double-fading attenuation. This study demonstrated the substantial potential of active RIS technology in enhancing WPCN performance. The results provide valuable insights for designing efficient and robust wireless communication systems that can leverage the capabilities of active RISs to achieve improved network efficiency and coverage. Active RISs are a transformative improvement in wireless communication technology, with the promise of a more capable and efficient wireless future.

Author Contributions: Conceptualization, I.H.; Formal analysis, I.H. and I.K.; Methodology, I.H.; Supervision, I.K.; Validation, I.H. and I.K.; Writing—original draft, I.H.; Writing—review & editing, I.H. and I.K. All authors have read and agreed to the published version of the manuscript.

Funding: This work was supported by “Regional Innovation Strategy (RIS)” through the National Research Foundation of Korea (NRF) funded by the Ministry of Education(MOE) (2021RIS-003).

Data Availability Statement: Data are contained within the article.

Conflicts of Interest: The authors declare no conflict of interest.

References

1. Chetri, L.; Bera, R. A Comprehensive Survey on Internet of Things (IoT) Toward 5G Wireless Systems. *IEEE Internet Things J.* **2020**, *7*, 16–32. [[CrossRef](#)]
2. Letaief, K.B.; Chen, W.; Shi, Y.; Zhang, J.; Zhang, Y.J.A. The Roadmap to 6G: AI Empowered Wireless Networks. *IEEE Commun. Mag.* **2019**, *57*, 84–90. [[CrossRef](#)]
3. Guo, F.; Yu, F.R.; Zhang, H.; Li, X.; Ji, H.; Leung, V.C.M. Enabling Massive IoT Toward 6G: A Comprehensive Survey. *IEEE Internet Things J.* **2021**, *8*, 11891–11915. [[CrossRef](#)]
4. Verma, S.; Kaur, S.; Khan, M.A.; Sehdev, P.S. Toward Green Communication in 6G-Enabled Massive Internet of Things. *IEEE Internet Things J.* **2021**, *8*, 5408–5415. [[CrossRef](#)]
5. Lu, X.; Wang, P.; Niyato, D.; Kim, D.I.; Han, Z. Wireless Networks with RF Energy Harvesting: A Contemporary Survey. *IEEE Commun. Surv. Tutor.* **2015**, *17*, 757–789. [[CrossRef](#)]
6. Bi, S.; Ho, C.K.; Zhang, R. Wireless Powered Communication: Opportunities and Challenges. *IEEE Commun. Mag.* **2015**, *53*, 117–125. [[CrossRef](#)]
7. Liu, X.; Qin, Z.; Gao, Y.; McCann, J.A. Resource Allocation in Wireless Powered IoT Networks. *IEEE Internet Things J.* **2019**, *6*, 4935–4945. [[CrossRef](#)]
8. Shi, W.; Wu, Q.; Xiao, F.; Shu, F.; Wang, J. Secrecy Throughput Maximization for IRS-Aided MIMO Wireless Powered Communication Networks. *IEEE Trans. Commun.* **2022**, *70*, 7520–7535. [[CrossRef](#)]

9. Ju, H.; Zhang, R. Throughput Maximization in Wireless Powered Communication Networks. *IEEE Trans. Wirel. Commun.* **2014**, *13*, 418–428. [[CrossRef](#)]
10. Bi, S.; Zeng, Y.; Zhang, R. Wireless powered communication networks: An overview. *IEEE Wirel. Commun.* **2016**, *23*, 10–18. [[CrossRef](#)]
11. Liu, X.; Xu, B.; Zheng, K.; Zheng, H. Throughput Maximization of Wireless-Powered Communication Network with Mobile Access Points. *IEEE Trans. Wirel. Commun.* **2023**, *22*, 4401–4415. [[CrossRef](#)]
12. Zheng, K.; Luo, R.; Wang, Z.; Liu, X.; Yao, Y. Short-Term and Long-Term Throughput Maximization in Mobile Wireless-Powered Internet of Things. *IEEE Internet Things J.* **2024**, *11*, 10575–10591. [[CrossRef](#)]
13. Lyu, T.; Xu, H.; Zhang, L.; Han, Z. Source Selection and Resource Allocation in Wireless-Powered Relay Networks: An Adaptive Dynamic Programming-Based Approach. *IEEE Internet Things J.* **2024**, *11*, 8973–8988. [[CrossRef](#)]
14. Tang, K.; Zheng, B.; Jiao, F.; Liu, X.; Feng, W.; Che, W.; Xue, Q. Joint Resource Allocation for Maximizing Energy Efficiency in MmWave-Based Wireless-Powered Communication Networks. *IEEE Trans. Veh. Technol.* **2024**, 1–15. [[CrossRef](#)]
15. Wu, Q.; Zhang, R. Towards Smart and Reconfigurable Environment: Intelligent Reflecting Surface Aided Wireless Network. *IEEE Commun. Mag.* **2020**, *58*, 106–112. [[CrossRef](#)]
16. Wu, Q.; Zhang, S.; Zheng, B.; You, C.; Zhang, R. Intelligent Reflecting Surface-Aided Wireless Communications: A Tutorial. *IEEE Trans. Commun.* **2021**, *69*, 3313–3351. [[CrossRef](#)]
17. Kisseleff, S.; Martins, W.A.; Al-Hraishawi, H.; Chatzinotas, S.; Ottersten, B. Reconfigurable Intelligent Surfaces for Smart Cities: Research Challenges and Opportunities. *IEEE Open J. Commun. Soc.* **2020**, *1*, 1781–1797. [[CrossRef](#)]
18. Cui, T.J.; Qi, M.Q.; Wan, X.; Zhao, J.; Cheng, Q. Coding metamaterials, digital metamaterials and programmable metamaterials. *Light Sci. Appl.* **2014**, *3*, e218. [[CrossRef](#)]
19. Cao, H.; Li, Z.; Chen, W. Resource Allocation for IRS-Assisted Wireless Powered Communication Networks. *IEEE Wirel. Commun. Lett.* **2021**, *10*, 2450–2454. [[CrossRef](#)]
20. Zheng, Y.; Bi, S.; Zhang, Y.J.; Quan, Z.; Wang, H. Intelligent Reflecting Surface Enhanced User Cooperation in Wireless Powered Communication Networks. *IEEE Wirel. Commun. Lett.* **2020**, *9*, 901–905. [[CrossRef](#)]
21. Wu, Q.; Zhang, R. Joint Active and Passive Beamforming Optimization for Intelligent Reflecting Surface Assisted SWIPT Under QoS Constraints. *IEEE J. Sel. Areas Commun.* **2020**, *38*, 1735–1748. [[CrossRef](#)]
22. Xu, D.; Yu, X.; Sun, Y.; Ng, D.W.K.; Schober, R. Resource Allocation for Secure IRS-Assisted Multiuser MISO Systems. In Proceedings of the 2019 IEEE Globecom Workshops (GC Wkshps), Waikoloa, HI, USA, 9–13 December 2019; pp. 1–6. [[CrossRef](#)]
23. Fang, F.; Xu, Y.; Pham, Q.V.; Ding, Z. Energy-Efficient Design of IRS-NOMA Networks. *IEEE Trans. Veh. Technol.* **2020**, *69*, 14088–14092. [[CrossRef](#)]
24. Li, Y.; Jiang, M.; Zhang, Q.; Qin, J. Joint beamforming design in multi-cluster MISO NOMA reconfigurable intelligent surface-aided downlink communication networks. *IEEE Trans. Commun.* **2020**, *69*, 664–674. [[CrossRef](#)]
25. Hameed, I.; Camana, M.R.; Tuan, P.V.; Koo, I. Intelligent Reflecting Surfaces for Sum-Rate Maximization in Cognitive Radio Enabled Wireless Powered Communication Network. *IEEE Access* **2023**, *11*, 16021–16031. [[CrossRef](#)]
26. Li, X.; Xie, Z.; Chu, Z.; Menon, V.G.; Mumtaz, S.; Zhang, J. Exploiting Benefits of IRS in Wireless Powered NOMA Networks. *IEEE Trans. Green Commun. Netw.* **2022**, *6*, 175–186. [[CrossRef](#)]
27. Di Renzo, M.; Ntontin, K.; Song, J.; Danufane, F.H.; Qian, X.; Lazarakis, F.; De Rosny, J.; Phan-Huy, D.T.; Simeone, O.; Zhang, R.; et al. Reconfigurable Intelligent Surfaces vs. Relaying: Differences, Similarities, and Performance Comparison. *IEEE Open J. Commun. Soc.* **2020**, *1*, 798–807. [[CrossRef](#)]
28. You, C.; Beixiong Zheng, W.M.; Zhang, R. How to Deploy Intelligent Reflecting Surfaces in Wireless Network: BS-side, User-side, or Both Sides? *J. Commun. Inf. Netw.* **2022**, *7*, 1. [[CrossRef](#)]
29. Han, Y.; Zhang, S.; Duan, L.; Zhang, R. Cooperative Double-IRS Aided Communication: Beamforming Design and Power Scaling. *IEEE Wirel. Commun. Lett.* **2020**, *9*, 1206–1210. [[CrossRef](#)]
30. Zheng, B.; You, C.; Zhang, R. Double-IRS Assisted Multi-User MIMO: Cooperative Passive Beamforming Design. *IEEE Trans. Wirel. Commun.* **2021**, *20*, 4513–4526. [[CrossRef](#)]
31. Han, Y.; Zhang, S.; Duan, L.; Zhang, R. Double-IRS Aided MIMO Communication Under LoS Channels: Capacity Maximization and Scaling. *IEEE Trans. Commun.* **2022**, *70*, 2820–2837. [[CrossRef](#)]
32. Mei, W.; Zhang, R. Cooperative Beam Routing for Multi-IRS Aided Communication. *IEEE Wirel. Commun. Lett.* **2021**, *10*, 426–430. [[CrossRef](#)]
33. Do, T.N.; Kaddoum, G.; Nguyen, T.L.; da Costa, D.B.; Haas, Z.J. Multi-RIS-Aided Wireless Systems: Statistical Characterization and Performance Analysis. *IEEE Trans. Commun.* **2021**, *69*, 8641–8658. [[CrossRef](#)]
34. Huo, Y.; Dong, X.; Ferdinand, N. Distributed Reconfigurable Intelligent Surfaces for Energy-Efficient Indoor Terahertz Wireless Communications. *IEEE Internet Things J.* **2023**, *10*, 2728–2742. [[CrossRef](#)]
35. Li, Z.; Hu, H.; Zhang, J.; Zhang, J. RIS-Assisted mmWave Networks with Random Blockages: Fewer Large RISs or More Small RISs? *IEEE Trans. Wirel. Commun.* **2023**, *22*, 986–1000. [[CrossRef](#)]
36. Li, Y.; You, C.; Chun, Y.J. Active-IRS Aided Wireless Network: System Modeling and Performance Analysis. *IEEE Commun. Lett.* **2023**, *27*, 487–491. [[CrossRef](#)]
37. Kang, Z.; You, C.; Zhang, R. Active-IRS-Aided Wireless Communication: Fundamentals, Designs and Open Issues. *IEEE Wirel. Commun.* **2024**, 1–7. [[CrossRef](#)]

38. Zhang, Z.; Dai, L.; Chen, X.; Liu, C.; Yang, F.; Schober, R.; Poor, H.V. Active RIS vs. Passive RIS: Which Will Prevail in 6G? *IEEE Trans. Commun.* **2023**, *71*, 1707–1725. [[CrossRef](#)]
39. Chen, G.; Wu, Q.; He, C.; Chen, W.; Tang, J.; Jin, S. Active IRS Aided Multiple Access for Energy-Constrained IoT Systems. *IEEE Trans. Wirel. Commun.* **2023**, *22*, 1677–1694. [[CrossRef](#)]
40. Zeng, P.; Qiao, D.; Wu, Q.; Wu, Y. Throughput maximization for active intelligent reflecting surface-aided wireless powered communications. *IEEE Wirel. Commun. Lett.* **2022**, *11*, 992–996. [[CrossRef](#)]
41. Dong, L.; Wang, H.M.; Bai, J. Active Reconfigurable Intelligent Surface Aided Secure Transmission. *IEEE Trans. Veh. Technol.* **2022**, *71*, 2181–2186. [[CrossRef](#)]
42. Zargari, S.; Hakimi, A.; Tellambura, C.; Herath, S. Multiuser MISO PS-SWIPT Systems: Active or Passive RIS? *IEEE Wirel. Commun. Lett.* **2022**, *11*, 1920–1924. [[CrossRef](#)]
43. Niu, H.; Lin, Z.; An, K.; Liang, X.; Hu, Y.; Li, D.; Zheng, G. Active RIS-Assisted Secure Transmission for Cognitive Satellite Terrestrial Networks. *IEEE Trans. Veh. Technol.* **2023**, *72*, 2609–2614. [[CrossRef](#)]
44. Long, R.; Liang, Y.C.; Pei, Y.; Larsson, E.G. Active Reconfigurable Intelligent Surface-Aided Wireless Communications. *IEEE Trans. Wirel. Commun.* **2021**, *20*, 4962–4975. [[CrossRef](#)]
45. Zhi, K.; Pan, C.; Ren, H.; Chai, K.K.; Elkashlan, M. Active RIS Versus Passive RIS: Which is Superior with the Same Power Budget? *IEEE Commun. Lett.* **2022**, *26*, 1150–1154. [[CrossRef](#)]
46. Hameed, I.; Koo, I. Exploiting Active-IRS by Maximizing Throughput in Wireless Powered Communication Networks. In *Advanced Intelligent Computing Technology and Applications, Proceedings of the International Conference on Intelligent Computing, Zhengzhou, China, 10–13 August 2023*; Huang, D.S., Premaratne, P., Jin, B., Qu, B., Jo, K.H., Hussain, A., Eds.; Springer: Singapore, 2023; pp. 367–376.
47. Wu, Q.; Zhou, X.; Schober, R. IRS-Assisted Wireless Powered NOMA: Do We Really Need Different Phase Shifts in DL and UL? *IEEE Wirel. Commun. Lett.* **2021**, *10*, 1493–1497. [[CrossRef](#)]
48. Zeng, M.; Nguyen, N.P.; Dobre, O.A.; Ding, Z.; Poor, H.V. Spectral- and Energy-Efficient Resource Allocation for Multi-Carrier Uplink NOMA Systems. *IEEE Trans. Veh. Technol.* **2019**, *68*, 9293–9296. [[CrossRef](#)]
49. Tse, D.; Viswanath, P. *Fundamentals of Wireless Communication*; Cambridge University Press: Cambridge, MA, USA, 2005.

Disclaimer/Publisher’s Note: The statements, opinions and data contained in all publications are solely those of the individual author(s) and contributor(s) and not of MDPI and/or the editor(s). MDPI and/or the editor(s) disclaim responsibility for any injury to people or property resulting from any ideas, methods, instructions or products referred to in the content.